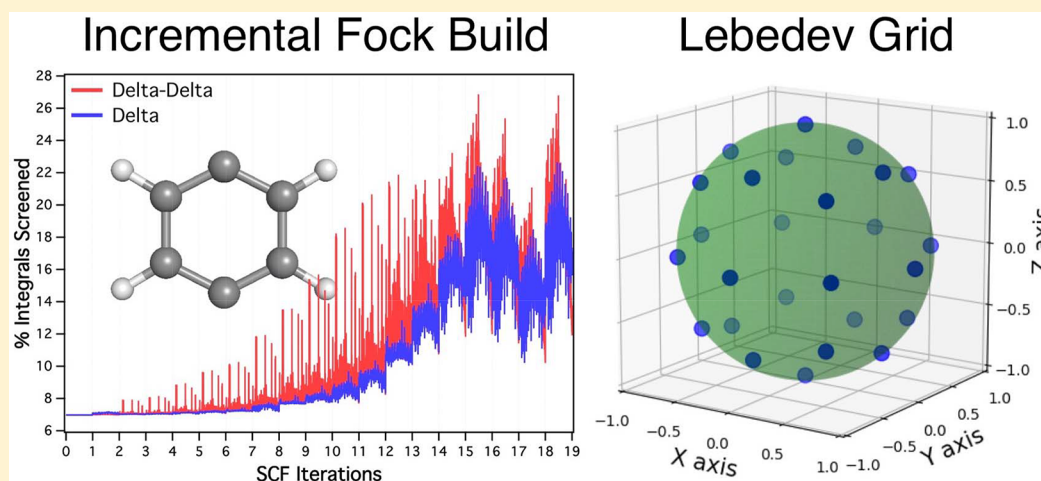


Efficient Implementation of Variation after Projection Generalized Hartree–Fock

Patrick J. Lestrage,[†] David B. Williams-Young,[†] Alessio Petrone,[†] Carlos A. Jiménez-Hoyos,[‡] and Xiaosong Li^{*,†}

[†]Department of Chemistry, University of Washington, Seattle, Washington 98195, United States

[‡]Department of Chemistry, Wesleyan University, Middletown, Connecticut 06459, United States



ABSTRACT: Projected Hartree–Fock (PHF) theory can restore important symmetries to broken symmetry wave functions. Variation after projection (VAP) implementations make it possible to deliberately break and then restore a given symmetry by directly minimizing the projected energy expression. This technique can be applied to any symmetry that can be broken from relaxing constraints on single Slater determinant wave functions. For instance, generalized Hartree–Fock (GHF) wave functions are eigenfunctions of neither \hat{S}_z nor S^2 . By relaxing these constraints, the wave function can explore a larger variational space and can reach lower energies than more constrained HF solutions. We have implemented spin-projected GHF (SGHF), which retains many of the advantages of breaking symmetry while also being a spin eigenfunction, with some notable improvements over previous implementations. Our new algorithm involves the formation of new intermediate matrices not previously discussed in the literature. Discretization of the necessary integration over the rotation group $SO(3)$ is also accomplished much more efficiently using Lebedev grids. A novel scheme to incrementally build rotated Fock matrices is also introduced and compared with more standard approaches.

1. INTRODUCTION

Strongly correlated systems present a unique challenge for electronic structure theory. These systems typically have degenerate or nearly degenerate orbitals which cause the single determinant description of the wave function to break down, leading to spontaneous symmetry breaking due to instabilities. While this symmetry breaking will lower the variational energy closer to the exact value, the approximate solution will not have the same symmetries as the true solution. On the other hand, if a solution is constrained to have the desired symmetries of the exact solution this will raise the solution's energy and can lead to qualitatively incorrect descriptions of the system. Löwdin referred to this as the “symmetry dilemma” where one must make a choice on whether to enforce a particular symmetry or find a lower energy broken symmetry solution.¹

This dilemma has motivated the development of various projection techniques to approximately or exactly restore symmetries of broken symmetry wave functions. In this way the energy is lowered by symmetry breaking and lowered further by restoring the desired symmetry. The approximate wave function and its properties are also made more similar to the true solution. The simplest scheme is to apply a projection operator after converging to a stable broken symmetry solution, referred to as projection after variation (PAV). This projected wave function is not variationally optimized making the evaluation of properties and derivatives quite complicated.^{2–4} PAV also has difficulties near regions of spontaneous symmetry breaking, which can lead to discontinuities in the potential

Received: August 3, 2017

Published: January 3, 2018

energy surface. Further, most PAV implementations only approximately restore spin symmetry, so there will still be unresolved contaminating states.⁵ These problems can be addressed by variationally optimizing the wave function in the presence of the projection operator, known as variation after projection (VAP).

The problems with PAV approaches led to the development of the Extended Hartree–Fock method.^{6,7} This is a VAP approach that uses Löwdin’s spin projection operator to remove components of the wave function not having the desired spin symmetry. While this method was successful in many respects, Löwdin’s projection operator led to exceedingly complicated SCF equations and was all but abandoned. Simpler operators that restore spin symmetry have since been developed, renewing interest in this body of work. Scuseria and co-workers revitalized VAP techniques in the quantum chemistry community by applying them to the Hartree–Fock–Bogoliubov (HFB) and HF wave functions.^{8,9} They broke and restored not only spin symmetry but also complex conjugation, point group, and particle number in the case of HFB wave functions. These contributions built off of a larger body of work on symmetry projection in the nuclear physics community.^{10–12} Projected Hartree–Fock (PHF) wave functions retain the advantages of broken symmetry wave functions, namely, the larger variational space, and also have the same symmetries as the exact solution. In other words, they provide a solution to the “symmetry dilemma”.

The PHF method accounts for the majority of static correlation, but there is still a significant portion of dynamic correlation that is unaccounted for. This motivated the development of many techniques to add dynamic correlation in much the same way as ordinary HF. Scuseria and co-workers have worked to combine symmetry projection with DFT while attempting to avoid double counting of electron correlation¹³ and have reformulated the spin-projected HF wave function in terms of a polynomial similarity transformation to form a spin-projected coupled cluster theory.^{14,15} Other groups have also combined spin-projected HF with many-body perturbation theory¹⁶ and configuration interaction.^{17,18} There have also been efforts to develop a spin-projected linear response formalism.¹⁹

The majority of the recent extensions of Scuseria’s original work on PHF have focused on spin-projected unrestricted HF (SUHF). Our work revisits spin-projected GHF (SGHF) and provides ways to efficiently construct the PHF effective Fock matrix. First, we present an algorithm that is easily parallelized and minimizes memory usage by forming new intermediate quantities. We also advocate using a Lebedev integration grid when discretizing the integration over rotation angles and discuss issues with convergence associated with sparse grids. Finally, we present a novel scheme to incrementally build all necessary rotated Fock matrices. These modifications greatly reduce the cost of optimizing SGHF wave functions and will make it possible to study larger molecular systems with this method. Some of these techniques can also be used with projected UHF and with other types of projection operators.

2. THEORY

Projected Hartree–Fock theory (PHF) describes the electronic wave function in terms of a transfer operator (or a sum of transfer operators) acting on a broken symmetry wave function^{20,21}

$$|\Psi_m^S\rangle = \hat{P}|\Phi\rangle = \sum_k f_k \hat{P}_{mk}^S |\Phi\rangle \quad (1)$$

where $|\Psi_m^S\rangle$ is a wave function with quantum numbers S and m . The coefficients f_k are determined by diagonalizing the Hamiltonian in the basis of the transfer operators. These operators are defined as linear combinations of group operators \hat{A} weighted by elements of the matrix associated with that operator in a particular irreducible representation

$$\hat{P}_{mk}^S = \frac{l_S}{h} \sum_{A \in G} \Gamma^S(A)_{mk}^* \hat{A} \quad (2)$$

The normalization factor l_S and h are the dimension of the irreducible representation Γ^S and the order of the group, respectively. These operators are meant to restore a particular symmetry such as spin, particle number, complex conjugation, or point group. The action of operator \hat{P}_{mk}^S produces a wave function that transforms as the m th row of irreducible representation Γ^S , thus having m and S as good quantum numbers. While these are not truly projection operators if $m \neq k$, they do achieve the goal of preparing a wave function with the desired quantum numbers.

The projected wave function is determined by minimizing the projected energy expression

$$E = \frac{\langle \Phi | \hat{H} \hat{P} | \Phi \rangle}{\langle \Phi | \hat{P} | \Phi \rangle} \quad (3)$$

where we have used the fact that \hat{P} commutes with the Hamiltonian and that it is idempotent. The specific form of \hat{P} and the representation of the broken symmetry wave function will dictate how to efficiently minimize this function.

2.1. Spin-Projection Operator. Spin symmetry can be restored by forcing the projected wave function to be invariant to the axis of spin quantitation.²² The operator that accomplishes this is expressed as

$$\begin{aligned} \hat{P}_{mk}^S &= |S; m\rangle \langle S; k| \\ &= \frac{2S+1}{8\pi^2} \int_0^{2\pi} \int_0^\pi \int_0^{2\pi} d\alpha d\beta d\gamma \\ &\quad \sin(\beta) D_{mk}^{S*}(\alpha, \beta, \gamma) e^{-i\alpha \hat{S}_z} e^{-i\beta \hat{S}_y} e^{-i\gamma \hat{S}_z} \end{aligned} \quad (4)$$

where $D_{mk}^S(\alpha, \beta, \gamma)$ is a Wigner rotation matrix element.^{23,24} The label S indicates the total spin of the projected wave function and m and k are different spin projections along the z -axis. This operator involves an integration over the rotation group $SO(3)$, and we will discuss how to efficiently discretize this integration in later sections. This work will focus exclusively on spin-projection as it has special significance in the context of chemical problems, but much of the later discussion is also applicable to the restoration of other symmetries as we will point out where appropriate.

2.2. Spin-Projected Hartree–Fock. The PHF energy for a particular spin symmetry is expressed as

$$E^S = \sum_{mk} f_m^* H_{mk} f_k \quad (5)$$

where the Hamiltonian matrix elements are

$$H_{mk} = \langle \Phi | \hat{H} \hat{P}_{mk}^S | \Phi \rangle \quad (6)$$

This matrix is of the dimension of the number of different spin projections $(2S + 1)$. The energy expression is a function of the broken symmetry density ρ formed from the broken symmetry molecular orbital coefficients

$$\rho_{\mu\nu} = \sum_i^{N_{\text{occ}}} C_{\mu i} C_{\nu i}^* \quad (7)$$

and the linear coefficients \mathbf{f} defining the expansion of the projected wave function in terms of transfer operators. The stationary conditions for this variational problem are determined from variations in the following Lagrangian under the constraints that the broken symmetry density remains idempotent and that the projected wave function is normalized

$$\begin{aligned} \mathcal{L}^S[\mathbf{f}, \rho] = & \sum_{mk} f_m^* H_{mk} f_k - \text{Tr}[\Lambda(\rho^2 - \rho)] \\ & - E^S \left(\sum_{mk} f_m^* W_{mk} f_k - \mathbf{1} \right) \end{aligned} \quad (8)$$

where we have introduced the projected overlap matrix elements

$$W_{mk} = \langle \Phi | \hat{P}_{mk}^S | \Phi \rangle \quad (9)$$

The stationary conditions resulting from variation of this Lagrangian with respect to the linear coefficients leads to the generalized eigenvalue problem

$$\mathbf{H}\mathbf{f} = \mathbf{W}\mathbf{f}E^S \quad (10)$$

This is a small configuration interaction (CI) problem in the basis of the different spin projections along the z -axis. The linear coefficients and the energy of the system are obtained by solving this problem. Variation of the Lagrangian with respect to the broken symmetry density leads to a familiar stationary condition

$$[\mathcal{F}, \rho] = \mathbf{0} \quad (11)$$

where \mathcal{F} is not the standard Fock matrix but an effective Fock matrix. This matrix is defined as

$$\mathcal{F} = \sum_{mk} f_m^* f_k \int dg w_{mk}(g) (\mathcal{F}_g - E^S \mathbf{X}_g) \quad (12)$$

where $w_{mk}(g)$ is a weight, \mathcal{F}_g is a matrix defined at a given rotation angle, and \mathbf{X}_g is related to the derivative of the overlap matrix \mathbf{W} . Explicit expressions for these terms can be found in the [Appendix](#) but are left out of this section for brevity. The above stationary condition can be satisfied by solving the PHF self-consistent field (SCF) equation

$$\mathcal{F}\mathbf{C} = \mathbf{C}\epsilon \quad (13)$$

in much the same way as for ordinary HF, but while also solving [eq 10](#) to obtain the linear coefficients every SCF iteration.

3. COMPUTATIONAL DETAILS

Spin-projected generalized Hartree–Fock has been implemented in the Chronus Quantum software package.²⁵ This implementation forms new intermediates not discussed in previous works and also takes a novel approach to incrementally forming Fock matrices.

The effective Fock matrix is a function of the linear coefficients \mathbf{f} , the energy E^S , and involves an integration over

the rotation angles g ([eq 12](#)). The Hamiltonian \mathbf{H} and overlap matrix \mathbf{W} are also formed by integrating over the rotation angles and are used to determine the linear coefficients and energy, so the effective Fock matrix cannot be completely formed until [eq 10](#) is solved during each SCF iteration.

One approach would be to form the Hamiltonian and overlap matrices, solve [eq 10](#), and then began the process of forming the effective Fock matrix. Code structured in this way would require many intermediate quantities used to form the Hamiltonian, overlap matrix, and effective Fock matrices to be stored in memory. These include all the rotated density matrices and rotated Fock matrices at each point in the integration over g (see the [Appendix](#) for explicit expressions). This structure also requires multiple loops over the integration grid, an undesirable condition if parallelizing over integration points. We can simplify the scheme and only loop over the integration grid once every SCF cycle by forming new intermediate matrices

$$\mathbf{F}_{mk} = \int dg w_{mk}(g) \mathcal{F}_g \quad (14)$$

$$\mathbf{X}_{mk} = \int dg w_{mk}(g) \mathbf{X}_g \quad (15)$$

The number of intermediate matrices scales with the size of the CI problem, so there will only be $(2S + 1)(2S + 2)/2$ matrices or the dimension of the lower triangle of the Hamiltonian. Although for the special case of singlet projection, the effective Fock matrix can be formed directly with no intermediate matrices being necessary. After this integration, we can solve [eq 10](#) to determine the linear coefficients and then contract them with these intermediate matrices to complete the formation of the effective Fock matrix. The general structure of this algorithm is presented in [Figure 1](#).

Build integration grid and determine grid weights

while SCF not converged **do**

 Transform the broken symmetry density to the NO basis

for $g = 0$ to N_{grid} **do**

 Form \mathbf{X}_g , and \mathcal{F}_g

for $m, k = 0$ to $2S + 1$ **do**

 | Add contributions to W_{mk} , H_{mk} , \mathbf{X}_{mk} , and \mathbf{F}_{mk}

end

end

 Solve the CI Problem

 Contract \mathbf{X}_{mk} and \mathbf{F}_{mk} with the CI vector

 Diagonalize \mathcal{F} and evaluate convergence

end

Figure 1. Schematic of the algorithm for spin-projected GHF.

This scheme is advantageous for several reasons. For one, this structure makes it simpler to limit memory usage in the case where all rotated densities, overlap matrices, and rotated Fock matrices cannot be stored in memory at one time, although this is an unlikely scenario on most modern machines. There are similar memory requirements for the incremental Fock build scheme to be presented later, but these intermediate matrices still remove any need to loop over the grid points more than once. Another advantage is that all integration points are independent, so the loop over g can easily be split over several cores and the collected quantities formed after each core has completed its task.

Table 1. Error of $\langle S^2 \rangle$ and Energy for Different Integration Grids^a

| molecule | basis set | grid | no. points | $\langle S^2 \rangle$ error | remaining spin cont. | energy error (E_h) |
|----------------|-----------|----------------------|------------|-----------------------------|--------------------------|------------------------|
| H ₃ | STO-3G | TrapGaussLeg(2,2,2) | 8 | 8.234×10^{-2} | 93.7% | 1.434×10^{-2} |
| | | TrapGaussLeg(2,6,2) | 24 | 1.279×10^{-5} | $1.45 \times 10^{-2}\%$ | 1.646×10^{-6} |
| | | TrapGaussLeg(2,10,2) | 40 | 2.808×10^{-12} | $3.20 \times 10^{-9}\%$ | |
| | | LebedevTrap(6,2) | 12 | | | |
| O ₂ | 6-31G | TrapGaussLeg(6,10,6) | 360 | 1.024×10^{-9} | $3.02 \times 10^{-6}\%$ | 1.91×10^{-10} |
| | | TrapGaussLeg(7,10,7) | 490 | -5.620×10^{-12} | $1.66 \times 10^{-8}\%$ | |
| | | LebedevTrap(14,6) | 84 | 8.760×10^{-10} | $2.58 \times 10^{-6}\%$ | 1.40×10^{-10} |
| | | LebedevTrap(26,7) | 182 | -7.017×10^{-14} | $2.07 \times 10^{-10}\%$ | |

^aNote that an optimized TrapGaussLeg algorithm may lead to a smaller number of grid points than in our implementation, but the LebedevTrap grid is still optimal in all cases.

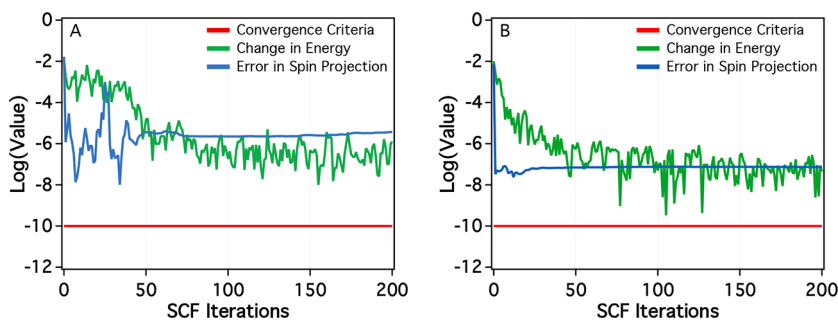


Figure 2. SGHF convergence behavior of triplet O₂ modeled with the 6-31G basis set with the TrapGaussLeg(6,6,6) (A) and TrapGaussLeg(8,8,8) (B) grids.

Spin projection operators involve an integration over the rotation group $SO(3)$, which must be discretized in some way. Previous implementations of SGHF advocated using a Trapezoid grid for integration over α and γ and a Gauss-Legendre grid for integration over β .⁸ These choices result in very dense integration grids since about 10 points for each angle are usually necessary to adequately restore spin symmetry. At each integration point, rotated Fock matrices need to be constructed, which is the most computationally expensive operation. Any reduction in the number of grid points should therefore significantly reduce the cost of a calculation.

The integration over $SO(3)$ can be broken down to two surface integrals over a 2-sphere S^2 and one over S^1 .²⁶ Lebedev integration grids discretize the surface integral of a 2-sphere and are commonly used when evaluating DFT exchange correlation functionals.^{27,28} All integration points lie on the surface of a unit sphere and are invariant under the octahedral rotation group with inversion. They are classified into different orders, where the order n grid integrates exactly all spherical harmonics of order n or less. Lebedev grids are efficient schemes to evaluate the surface integral of a unit sphere and can be used to integrate over the α (or γ) and β rotation angles for spin-projected GHF. Compared to the mixed Trapezoid and Gauss-Legendre grid, far fewer integration points are required to achieve the same accuracy in spin symmetry restoration. Our implementation uses a Lebedev grid for integration over S^2 (α and β) and a Trapezoid grid for integration over S^1 (γ).

4. RESULTS AND DISCUSSION

4.1. Lebedev Grid. We have compared two different schemes to discretize the spin-projection operator. The first scheme uses a Trapezoid grid for α and γ and a Gauss-Legendre grid for β denoted as TrapGaussLeg($n_\alpha, n_\beta, n_\gamma$) and the second uses a Lebedev grid for α and β with a Trapezoid grid for γ

denoted as LebedevTrap($n_{\alpha\beta}, n_\gamma$). Table 1 shows the error in spin symmetry restoration and the error in the converged energy relative to a denser grid that yields the lowest energy solution. All calculations begin with a converged UHF or GHF solution as the initial guess for the SGHF calculation. The percent error of $\langle S^2 \rangle$ relative to that of the starting UHF/GHF solution is also included to show the percentage of the starting spin contamination remaining as a measure of the quality of the spin projection.

Our comparison aims to determine the smallest grid required to restore the desired spin symmetry with an error $< 1.0 \times 10^{-10}$ (the energy convergence criteria in these calculations). In Table 1 the largest grid in each category is the smallest grid that meets this criteria. For H₃ the atoms were arranged in an equilateral triangle with 1 Å separation. The broken symmetry GHF solution has $\langle S^2 \rangle = 0.838$ and spin projection restores the system to doublet symmetry. The O₂ bond length was optimized with UHF and the 6-31G basis set ($\langle S^2 \rangle = 2.034$) using the Gaussian16 software package³⁰ and the projection operator restores triplet symmetry.

Minimal basis H₃ is an extreme example illustrating the benefit of Lebedev grids as the smallest Lebedev and Trapezoid grids achieve perfect spin symmetry restoration within machine epsilon. The LebedevTrap(6,2) grid has ~ 3.33 times fewer grid points than the TrapGaussLeg(2,10,2) grid, but does a better job of restoring the system to doublet symmetry. Both grids converge to the same energy within the convergence criteria, so no errors are reported. The smaller TrapGaussLeg grids show comparable errors in spin symmetry restoration to that of the converged energy. For O₂ with the 6-31G basis set, ~ 2.7 times fewer points are required when using a Lebedev grid. These calculations are representative of the savings seen for other systems.

There are two notable problems that can arise when the integration grid is not dense enough. The first is that the error

in forming the overlap matrix (eq 9) may be so great that it is not positive definite, making the generalized eigenvalue problem in eq 10 ill-defined. The other problem concerns convergence when the integration error is greater than or comparable to the convergence criteria. Both of these problems present themselves when modeling triplet O₂. The overlap matrix is not positive definite when using the LebedevTrap-(6,6) grid although an even smaller grid was successful at restoring spin symmetry for H₃. The three grids presented in Table 1 all converge in 12 SCF iterations, but smaller grids oscillate about the correct energy when the error in symmetry restoration is greater than the convergence criteria. Figure 2 shows the convergence behavior for smaller integration grids that did not converge within 200 iterations despite using the same initial guess and optimization scheme as the grids in Table 1.

The error in spin symmetry restoration may dictate whether self-consistency can be reached and should be used to determine whether a denser integration grid is necessary. This also means that sparser integration grids can likely be used if the energy convergence criteria are looser. This has implications beyond just spin-projection and should be an important consideration when using other projection operators that require discretization of an integration, such as when restoring particle number symmetry for HFB wave functions.

4.2. Incremental Fock Build. During the PHF SCF procedure, a rotated Fock matrix needs to be formed at each grid point in the integration over the rotation angles

$$\mathbf{F}[\rho_g] = \mathbf{h} + \mathbf{G}[\rho_g] \quad (16)$$

where \mathbf{h} is the core Hamiltonian and $\mathbf{G}[\rho_g]$ is the perturbation tensor defined as

$$(\mathbf{G}[\rho_g])_{ij} = \sum_{kl} \langle ik||jl \rangle (\rho_g)_{lk} \quad (17)$$

and $\langle ik||jl \rangle$ are antisymmetrized two-electron integrals. We can take advantage of the fact that this matrix is linear in the density to more effectively screen two-electron integrals and reduce the cost of forming this matrix.

For ordinary HF, if the two-electron integrals cannot be stored in memory (or if writing/reading them from disk is too slow) they can be computed directly at each SCF iteration when forming the perturbation tensor. It is often advantageous to incrementally form the Fock matrix by only calculating the change in \mathbf{G} at SCF iteration k

$$\mathbf{F}[\rho^k] = \mathbf{F}[\rho^{k-1}] + \mathbf{G}[\Delta\rho^k] \quad (18)$$

where the density difference is $\Delta\rho^k = \rho^k - \rho^{k-1}$. The two-electron integrals used to form $\mathbf{G}[\Delta\rho^k]$ can be screened more effectively since the density difference should be very small between SCF cycles and will approach zero as the calculation nears convergence.³¹ For instance, the two-electron integrals used to construct \mathbf{G} can be screened using the Schwartz inequality

$$\langle ij|kl \rangle \rho_{ij} \leq \sqrt{\langle ij||ij \rangle} \sqrt{\langle kl||kl \rangle} \rho_{ij} \quad (19)$$

If the RHS of the above equation is below a particular threshold, then the $\langle ij|kl \rangle$ integral does not need to be evaluated as its contribution will not be significant. Obviously more integrals will fall below a given threshold and can be screened out if the argument to \mathbf{G} is smaller.

This same approach can be used to build the rotated Fock matrices in eq 16. All the rotated Fock matrices and all the density differences at each integration point can be stored and used to update the rotated Fock matrix during the next SCF cycle. A rotated Fock matrix at SCF cycle k can be calculated as

$$\mathbf{F}[\rho_g^k] = \mathbf{F}[\rho_g^{k-1}] + \mathbf{G}[\Delta\rho_g^k] \quad (20)$$

where $\Delta\rho_g^k = \rho_g^k - \rho_g^{k-1}$. In the case where all these integral contractions were being done simultaneously, the mechanism for screening integrals is not clear. All ρ_g will not have the same screening profiles, so choosing any single density to screen all others would likely lead to large errors in the Fock formation. It should also be noted that storing many rotated matrices every SCF cycle does require a nontrivial amount of memory. However, on modern compute clusters and with the smaller grids presented in the previous section, this likely will not be an issue in most cases. Also this memory requirement is certainly smaller than that required to store all two-electron integrals in-core (the constraint that would prompt one to directly build Fock matrices).

For spin-projected HF, not only should densities be very similar between each SCF iteration, but many of the rotated densities at each SCF iteration should also be very similar to one another. This can be leveraged to screen even more integrals during the construction of each Fock matrix. Rotated Fock matrices can thus be built incrementally as

$$\mathbf{F}[\rho_g^k] = \mathbf{F}[\rho_{g'}^{k-1}] + \mathbf{G}[\rho_{g'}^k] - \mathbf{G}[\rho_{g'}^{k-1}] + \mathbf{G}[\Delta\Delta\rho_g^k] \quad (21)$$

where g' denotes the previously evaluated grid point before g and the density difference

$$\begin{aligned} \Delta\Delta\rho_g^k &= \Delta\rho_g^k - \Delta\rho_{g'}^k \\ &= (\rho_g^k - \rho_g^{k-1}) - (\rho_{g'}^k - \rho_{g'}^{k-1}) \end{aligned} \quad (22)$$

is between two SCF iterations and between two grid points. For this scheme to be advantageous, the rotated density matrices at consecutively evaluated grid points must be very similar. This is not guaranteed to be the case for any random ordering, so the grid points must be sorted to achieve this end. Unfortunately, sorting grid points to be in an optimal ordering is equivalent to solving the NP-hard traveling salesman problem.³² This is obviously impractical and we have opted to use the greedy nearest neighbor approach to highlight the potential of this approach.³³ After the first SCF iteration, the differences between each rotated density are evaluated and the grid points are reordered to minimize the differences between consecutively evaluate grid points. Future works will attempt more optimal solutions to this problem, but this simple solution is sufficient to showcase the utility of the approach.

We have optimized the SGHF triplet wave function of *p*-benzene with the STO-3G basis set and the LebedevTrap-(50,10) grid using both screening approaches. The molecular geometry was optimized at the UHF/STO-3G level of theory with the Gaussian16 software package. When using the $\Delta\Delta\rho_g^k$ matrix to incrementally build the Fock matrix we screen either significantly more integrals, a comparable number, or marginally fewer integrals than using $\Delta\rho_g^k$ (Figure 3). We have denoted the two approaches as “Delta” and “Delta–Delta” density screening. At some grid points in the early SCF iterations, twice as many integrals are screened using the Delta–Delta density during the formation of the perturbation tensor. Although, the

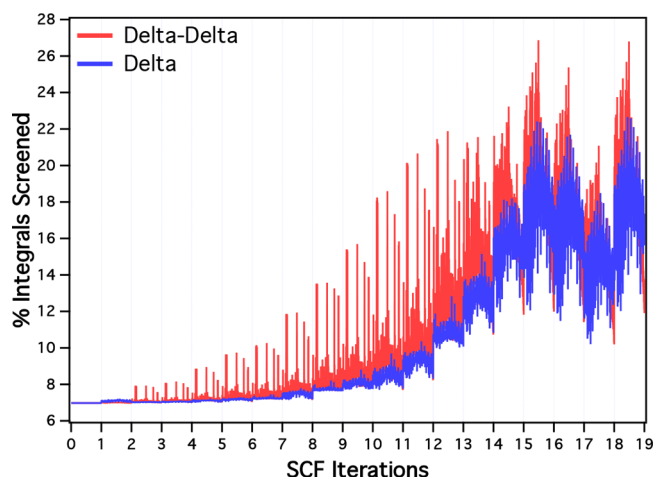


Figure 3. Percentage of two-electron integrals screened during the construction of each Fock matrix for triplet *p*-benzyne using the STO-3G basis and a LebedevTrap(50,10) grid. Using $\Delta\Delta\rho_g^k$ (Delta–Delta) is either significantly better, comparable, or only marginally worse than screening using $\Delta\rho_g^k$ (Delta).

changes in the number of screened integrals at each grid point also vary more dramatically using the Delta–Delta density. This is likely due to the particular order in which the grid points are evaluated and should change with a different ordering of the grid points. The advantages of this new approach are diminished near convergence where the norm of $\Delta\rho_g^k$ approaches that of $\Delta\Delta\rho_g^k$ and very near convergence these two approaches are comparable in how effectively they screen two-electron integrals. These results suggest that we should expect significant computational savings using this approach for larger molecular systems.

Radical polyacetylene chains of increasing length illustrate how large percentages of integrals can be screened by incrementally building the Fock matrix. As the spatial extent of the molecules increases, so does the percentage of integrals screened. The doublet SGHF wave function of two, four, six, and eight carbon chains have been optimized with the 6-31G basis set and the LebedevTrap(26,8) grid. Figure 4 shows that the Delta–Delta approach continues to follow the screening achieved by the Delta approach as the system size increases. It also continues to screen more integrals, a comparable amount, or only marginally fewer than those screened by the Delta approach. It should be noted that the cases where the Delta–Delta approach screens fewer integrals could be addressed by switching to the Delta approach based on the respective norms of the difference densities. In this way an optimal integral screening can be achieved for every Fock matrix formation.

There is also an alternative approach to using $\Delta\rho_g^k$ or $\Delta\Delta\rho_g^k$ that could be advantageous in some cases. The density difference could instead be defined relative to the true PHF density from the previous iteration

$$\Delta\tilde{\rho}_g^k = \rho_g^k - \sum_{ml} f_m^* f_l \int dg' w_{ml}(g') \rho_g^{k-1} \quad (23)$$

Memory requirements would be about half of what is required for the Delta or Delta–Delta schemes. All rotated Fock matrices from the previous iteration $F[\rho_g^{k-1}]$ would need to be stored, but the density matrices from the previous iteration would not be. The fully integrated PHF density could be formed and stored during the previous iteration without

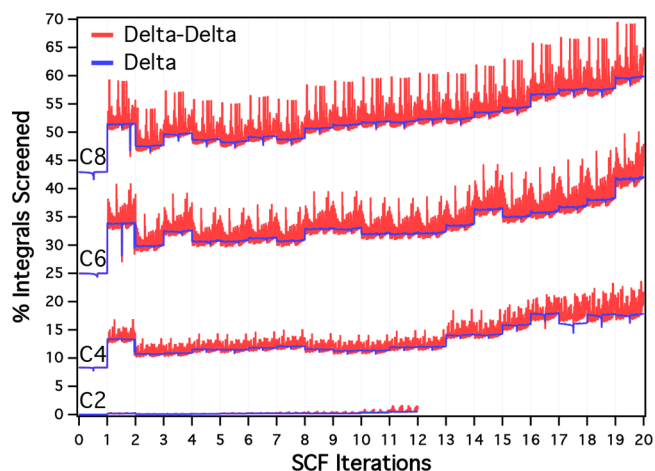


Figure 4. Percentage of two-electron integrals screened during the construction of each Fock matrix for doublet polyacetylene chains using the 6-31G basis and a LebedevTrap(26,8) grid. The two, four, six, and eight carbon chains are included. The $\Delta\Delta\rho_g^k$ (Delta–Delta) approach continues to track the screening achieved by the $\Delta\rho_g^k$ (Delta) approach and outperforms in many cases.

needing to store the densities at each grid point. For most calculations with hundreds to thousands of basis functions on modern compute clusters, the Delta or Delta–Delta schemes would still be the preferred choices. However, there are likely limiting cases where memory constraints would require using the density difference in eq 23.

These schemes can still be parallelized over integration points. There are no additional considerations for the Delta approach and the approach in eq 23 as they only require information from the previous SCF iteration. The Delta–Delta approach, on the other hand, must have information from the previously evaluated grid point of the current SCF iteration. This approach can still be used if the grid points are split into batches across different processors, as the grid points in those batches will still be evaluated consecutively and can use information from the previous grid point. If the number of processors is the same as or greater than the number of grid points, then the Delta–Delta approach cannot be used. In this case all grid points would be evaluated at the same time and the standard Delta density approach could still be used. The need to calculate two-electron integrals at each grid point for the Delta–Delta approach to achieve optimal screening is prohibitive in many cases and would not always be outweighed by the improved integral screening and accuracy. The ordinary Delta approach and the alternative scheme in eq 23 avoid this problem by being able to contract with the densities at each grid point simultaneously. Although, how to effectively define the screening criteria for so many densities with different profiles would need to be investigated further.

5. CONCLUSIONS

Spin-projected Hartree–Fock is a powerful technique for describing molecular systems with a desired spin symmetry. It retains many of the advantages of broken symmetry solutions, such as having lower energy than more constrained solutions while also preserving spin as a good quantum number. By projecting out contaminating spin states, this addresses the well-known “symmetry dilemma” and still scales as a mean-field approach.

This work builds off of previous developments from Scuseria and co-workers to develop an efficient scheme to build the effective Fock matrix of spin-projected generalized Hartree–Fock. We have developed an algorithm that forms intermediate matrices not previously discussed in the literature. We also advocate using Lebedev integration grids to discretize the integration over $SO(3)$ when restoring spin symmetry. Far fewer grid points are required than previously proposed grids to achieve the same accuracy in spin symmetry restoration. Our investigation of different integration grids also revealed that the error in spin symmetry restoration can create a soft bound on the energy convergence. This means that an appropriate integration grid can be determined based on the SCF convergence criteria. We have also presented a novel way to incrementally build rotated Fock matrices in PHF using density differences between two different SCF iterations and between two grid points. This scheme shows significant improvements in integral screening over just using the density difference between two SCF iterations. These improvements should make it possible to study more complex molecular systems with spin-projected GHF.

APPENDIX

This section provides explicit expressions for all terms presented in Figure 1 and walks through each step of the algorithm in detail. This implementation of projected Hartree–Fock requires using matrices in the atomic orbital (AO), orthonormal atomic orbital (OAO), and the natural orbital (NO) bases. Matrices in the OAO basis are denoted with a prime, and those in the NO basis have a tilde to differentiate them from AO basis matrices.

The first step is to combine the grid weights at each integration point with the Wigner D-matrix elements for all necessary spin-projections m and k

$$x(\alpha, \beta, \gamma)_{mk} = G(\alpha, \beta, \gamma) D_{mk}^{S^*}(\alpha, \beta, \gamma) \quad (24)$$

where $G(\alpha, \beta, \gamma)$ is the weight at a particular grid point. In the following discussion each grid point will be denoted by $g = (\alpha, \beta, \gamma)$. These quantities can be formed once and used throughout the SCF procedure.

The broken symmetry density must be transformed to the NO basis. The AO density matrix is first transformed to the OAO basis using the transformation matrix \mathbf{T} .

$$\rho^{\sigma\tau} = \mathbf{C}_{occ}^{\sigma} \mathbf{C}_{occ}^{\tau\dagger} \quad (25)$$

$$\rho = \begin{pmatrix} \rho^{\alpha\alpha} & \rho^{\alpha\beta} \\ \rho^{\beta\alpha} & \rho^{\beta\beta} \end{pmatrix} \quad (26)$$

$$\rho' = \begin{pmatrix} \mathbf{T}^\dagger & \mathbf{0} \\ \mathbf{0} & \mathbf{T}^\dagger \end{pmatrix} \begin{pmatrix} \rho^{\alpha\alpha} & \rho^{\alpha\beta} \\ \rho^{\beta\alpha} & \rho^{\beta\beta} \end{pmatrix} \begin{pmatrix} \mathbf{T} & \mathbf{0} \\ \mathbf{0} & \mathbf{T} \end{pmatrix} \quad (27)$$

The OAO density matrix is then diagonalized, and the NO transformation matrix \mathbf{O} (formed from the eigenvectors from diagonalizing the OAO density) is used during the current SCF iteration.

$$\tilde{\rho} = \mathbf{O}^\dagger \rho' \mathbf{O} \quad (28)$$

$$= \begin{pmatrix} \tilde{\rho}_{oo} & \tilde{\rho}_{ov} \\ \tilde{\rho}_{vo} & \tilde{\rho}_{vv} \end{pmatrix} = \begin{pmatrix} \mathbf{1} & \mathbf{0} \\ \mathbf{0} & \mathbf{0} \end{pmatrix} \quad (29)$$

Note that in the AO and OAO bases the density matrix is spin blocked, but in the NO basis it has occupied and virtual blocks.

At this point, we start the loop over all grid points g . The rotation matrix is constructed from three separate matrices defined by each rotation angle. This is trivially done in the OAO basis and then transformed to the NO basis.

$$\mathbf{R}'_g = \mathbf{R}'(\alpha, \hat{S}_z) \mathbf{R}'(\beta, \hat{S}_y) \mathbf{R}'(\gamma, \hat{S}_z) \quad (30)$$

$$\mathbf{R}'(\alpha, \hat{S}_z) = \begin{pmatrix} e^{i\alpha/2} \mathbf{1} & \mathbf{0} \\ \mathbf{0} & e^{-i\alpha/2} \mathbf{1} \end{pmatrix} \quad (31)$$

$$\mathbf{R}'(\beta, \hat{S}_y) = \begin{pmatrix} \cos(\beta/2) \mathbf{1} & \sin(\beta/2) \mathbf{1} \\ -\sin(\beta/2) \mathbf{1} & \cos(\beta/2) \mathbf{1} \end{pmatrix} \quad (32)$$

$$\tilde{\mathbf{R}}'_g = \mathbf{O}^\dagger \mathbf{R}'_g \mathbf{O} \quad (33)$$

The overlap between the broken symmetry determinant and the rotated determinant can now be evaluated using the rotation matrix and the NO density. This can then be used to renormalize the grid weights determined above.

$$\tilde{\mathbf{N}}_g = \left[(\tilde{\rho}_{oo} \quad \tilde{\rho}_{ov}) \tilde{\mathbf{R}}'_g \begin{pmatrix} \tilde{\rho}_{oo} \\ \tilde{\rho}_{vo} \end{pmatrix} \right]^{-1} \quad (34)$$

$$w_{mk}(g) = x_{mk}(g) / \det(\tilde{\mathbf{N}}_g \tilde{\rho}_{oo}) \quad (35)$$

The rotated density matrix in the NO basis can now be constructed.

$$\tilde{\rho}_g = \tilde{\mathbf{R}}'_g \begin{pmatrix} \tilde{\rho}_{oo} \\ \tilde{\rho}_{vo} \end{pmatrix} \tilde{\mathbf{N}}_g \begin{pmatrix} \tilde{\rho}_{oo} & \tilde{\rho}_{ov} \end{pmatrix} \quad (36)$$

The rotated density matrix is then used to construct the rotated Fock matrix. This is formed in the AO basis and then transformed back to the NO basis.

$$\rho'_g = \mathbf{O} \tilde{\rho}_g \mathbf{O}^\dagger \quad (37)$$

$$\begin{pmatrix} \rho'_g{}^{\alpha\alpha} & \rho'_g{}^{\alpha\beta} \\ \rho'_g{}^{\beta\alpha} & \rho'_g{}^{\beta\beta} \end{pmatrix} = \begin{pmatrix} \mathbf{T} & \mathbf{0} \\ \mathbf{0} & \mathbf{T} \end{pmatrix} \begin{pmatrix} \rho'_g{}^{\alpha\alpha} & \rho'_g{}^{\alpha\beta} \\ \rho'_g{}^{\beta\alpha} & \rho'_g{}^{\beta\beta} \end{pmatrix} \begin{pmatrix} \mathbf{T}^\dagger & \mathbf{0} \\ \mathbf{0} & \mathbf{T}^\dagger \end{pmatrix} \quad (38)$$

$$(\mathbf{G}'_g)_{ij} = \delta_{\sigma\tau} \sum_{kl} \langle iklj | \rangle (\rho_g^{\alpha\alpha})_{lk} + (\rho_g^{\beta\beta})_{lk} - \sum_{kl} \langle iklj | \rangle (\rho_g^{\sigma\tau})_{lk} \quad (39)$$

$$\mathbf{G}'_g = \begin{pmatrix} \mathbf{T}^\dagger & \mathbf{0} \\ \mathbf{0} & \mathbf{T}^\dagger \end{pmatrix} \begin{pmatrix} \mathbf{G}'_g{}^{\alpha\alpha} & \mathbf{G}'_g{}^{\alpha\beta} \\ \mathbf{G}'_g{}^{\beta\alpha} & \mathbf{G}'_g{}^{\beta\beta} \end{pmatrix} \begin{pmatrix} \mathbf{T} & \mathbf{0} \\ \mathbf{0} & \mathbf{T} \end{pmatrix} \quad (40)$$

$$\tilde{\mathbf{G}}_g = \mathbf{O}^\dagger \mathbf{G}'_g \mathbf{O} \quad (41)$$

$$\tilde{\mathbf{F}}_g = \tilde{\mathbf{h}} + \tilde{\mathbf{G}}_g \quad (42)$$

We now have all the necessary quantities to build the CI matrix elements by looping over the different spin projections m, k . Note that this step is not necessary for singlet states since the spin projection is always 0. We can update W_{mk} , H_{mk} , \mathbb{X}_{mk} , and F_{mk} for the current grid point.

$$W_{mk} += w_{mk}(g) \quad (43)$$

$$H_{mk} += \frac{1}{2} w_{mk}(g) [\text{Tr}[(\tilde{\mathbf{h}} + \tilde{\mathbf{F}}_g) \tilde{\rho}_g]] \quad (44)$$

$$\tilde{\mathbb{X}}_{mk} += w_{mk}(g) \tilde{\mathbb{X}}_g \quad (45)$$

$$\tilde{\mathbb{X}}_g = \tilde{\mathbf{R}}_g \begin{pmatrix} \tilde{\rho}_{oo} \\ \tilde{\rho}_{vo} \end{pmatrix} \tilde{\mathbf{N}}_g + \tilde{\mathbf{N}}_g \begin{pmatrix} \tilde{\rho}_{oo} & \tilde{\rho}_{ov} \end{pmatrix} \tilde{\mathbf{R}}_g \quad (46)$$

$$\tilde{F}_{mk} += w_{mk}(g) \tilde{\mathcal{F}}_g \quad (47)$$

$$\begin{aligned} \tilde{\mathcal{F}}_g = & \frac{1}{2} \tilde{\mathbb{X}}_g \text{Tr}[(\tilde{\mathbf{h}} + \tilde{\mathbf{F}}_g) \tilde{\rho}_g] + \tilde{\mathbf{N}}_g \begin{pmatrix} \tilde{\rho}_{oo} & \tilde{\rho}_{ov} \end{pmatrix} \tilde{\mathbf{F}}_g (\mathbf{1} - \tilde{\rho}_g) \tilde{\mathbf{R}}_g \\ & + (\mathbf{1} - \tilde{\rho}_g) \tilde{\mathbf{F}}_g \tilde{\mathbf{R}}_g \begin{pmatrix} \tilde{\rho}_{oo} \\ \tilde{\rho}_{vo} \end{pmatrix} \tilde{\mathbf{N}}_g \end{aligned} \quad (48)$$

The CI problem can now be solved to obtain the linear coefficients and energy. These can then be contracted with \mathbb{X}_{mk} and F_{mk} to finish forming the effective Fock matrix

$$\mathbf{Hf} = \mathbf{WfE}^S \quad (49)$$

$$\tilde{\mathcal{F}} = \sum_{mk} f_{mk}^* (\tilde{F}_{mk} - E^S \tilde{\mathbb{X}}_{mk}) \quad (50)$$

The occupied–occupied and virtual–virtual blocks of the effective Fock matrix are always 0, and at convergence the off-diagonal blocks vanish as well due to the Brillouin condition (eq 11). To ensure smooth convergence and separation of the occupied and virtual spaces, the diagonal blocks of the effective Fock matrix can be modified to use the blocks of the broken symmetry Fock matrix. The choice was proposed by Scuseria and co-workers and has proven to be effective in practice.

$$\tilde{\mathcal{F}} = \begin{pmatrix} \mathbf{0} & \tilde{\mathcal{F}}_{ov}^{PHF} \\ \tilde{\mathcal{F}}_{vo}^{PHF} & \mathbf{0} \end{pmatrix} \rightarrow \begin{pmatrix} \tilde{\mathbf{F}}_{oo}^{GHF} & \tilde{\mathcal{F}}_{ov}^{PHF} \\ \tilde{\mathcal{F}}_{vo}^{PHF} & \tilde{\mathbf{F}}_{vv}^{GHF} \end{pmatrix} \quad (51)$$

The effective Fock matrix can then be transformed to the OAO basis, diagonalized, and convergence evaluated. If the system has not converged, we return to the step where the broken symmetry density is transformed to the NO basis and proceed through the other steps until convergence is reached.

AUTHOR INFORMATION

Corresponding Author

*(X.L.) E-mail: xsl@uw.edu.

ORCID

David B. Williams-Young: 0000-0003-2735-3706

Xiaosong Li: 0000-0001-7341-6240

Funding

This research is funded by the U.S. Department of Energy (DE-SC0006863 to X.L.). The development of the Chronus Quantum open-source computational code is supported by

the NSF Office of Advanced Cyberinfrastructure (OAC-1663636 and CHE-1565520 to X.L.). Computations were facilitated through the use of advanced computational, storage, and networking infrastructure provided by the Hyak super-computer system at the University of Washington, funded by the Student Technology Fee, and the National Science Foundation (MRI-1624430).

Notes

The authors declare no competing financial interest.

ACKNOWLEDGMENTS

The authors would like to thank Gustavo Scuseria and Jeppe Olsen for stimulating discussions and for their insight.

REFERENCES

- (1) Lykos, P.; Pratt, G. W. Discussion on the Hartree-Fock Approximation. *Rev. Mod. Phys.* **1963**, *35*, 496–501.
- (2) McDouall, J. J.; Schlegel, H. B. Analytical Gradients for Unrestricted Hartree-Fock and Second Order Møller-Plesset Perturbation Theory with Single Ppin Annihilation. *J. Chem. Phys.* **1989**, *90*, 2363–2369.
- (3) Hratchian, H. P. Communication: An Efficient Analytic Gradient Theory for Approximate Spin Projection Methods. *J. Chem. Phys.* **2013**, *138*, 101101.
- (4) Thompson, L. M.; Hratchian, H. P. Second Derivatives for Approximate Spin Projection Methods. *J. Chem. Phys.* **2015**, *142*, 054106.
- (5) Schlegel, H. B. Potential Energy Curves using Unrestricted Møller-Plesset Perturbation Theory with Spin Annihilation. *J. Chem. Phys.* **1986**, *84*, 4530–4534.
- (6) Löwdin, P.-O. Quantum Theory of Many-particle Systems. II. Study of the Ordinary Hartree-Fock Approximation. *Phys. Rev.* **1955**, *97*, 1490–1508.
- (7) Mayer, I. The Spin-projected Extended Hartree-Fock Method. *Adv. Quantum Chem.* **1980**, *12*, 189–262.
- (8) Scuseria, G. E.; Jiménez-Hoyos, C. A.; Henderson, T. M.; Samanta, K.; Ellis, J. K. Projected Quasiparticle Theory for Molecular Electronic Structure. *J. Chem. Phys.* **2011**, *135*, 124108.
- (9) Jiménez-Hoyos, C. A.; Henderson, T. M.; Tsuchimochi, T.; Scuseria, G. E. Projected Hartree-Fock theory. *J. Chem. Phys.* **2012**, *136*, 164109.
- (10) Schmid, K. W.; Grümmer, F.; Faessler, A. Hartree-Fock-Bogoliubov Theory with Spin and Number Projection Before the Variation: An Application to ^{20}Ne and ^{22}Ne . *Nucl. Phys. A* **1984**, *431*, 205–229.
- (11) Sheikh, J. A.; Ring, P. Symmetry-projected Hartree-Fock-Bogoliubov Equations. *Nucl. Phys. A* **2000**, *665*, 71–91.
- (12) Sugimoto, S.; Ikeda, K.; Toki, H. Charge- and Parity-projected Hartree-Fock Method for the Strong Tensor Correlation and its Application to the Alpha Particle. *Nucl. Phys. A* **2004**, *740*, 77–94.
- (13) Garza, A. J.; Jiménez-Hoyos, C. A.; Scuseria, G. E. Electronic Correlation without Double Counting via a Combination of Spin Projected Hartree-Fock and Density Functional Theories. *J. Chem. Phys.* **2014**, *140*, 244102.
- (14) Wahlen-Strothman, J. M.; Henderson, T. M.; Hermes, M. R.; Degroote, M.; Qiu, Y.; Zhao, J.; Dukelsky, J.; Scuseria, G. E. Merging Symmetry Projection Methods with Coupled Cluster Theory: Lessons from the Lipkin Model Hamiltonian. *J. Chem. Phys.* **2017**, *146*, 054110.
- (15) Qiu, Y.; Henderson, T. M.; Scuseria, G. E. Projected Hartree-Fock Theory as a Polynomial of Particle-hole Excitations and its Combination with Variational Coupled Cluster Theory. *J. Chem. Phys.* **2017**, *146*, 184105.
- (16) Tsuchimochi, T.; Van Voorhis, T. Extended Møller-Plesset Perturbation Theory for Dynamical and Static Correlations. *J. Chem. Phys.* **2014**, *141*, 164117.

- (17) Tsuchimochi, T.; Ten-no, S. Communication: Configuration Interaction Combined with Spin-projection for Strongly Correlated Molecular Electronic Structures. *J. Chem. Phys.* **2016**, *144*, 011101.
- (18) Tsuchimochi, T.; Ten-no, S. Black-Box Description of Electron Correlation with the Spin-Extended Configuration Interaction Model: Implementation and Assessment. *J. Chem. Theory Comput.* **2016**, *12*, 1741–1759.
- (19) Tsuchimochi, T.; Van Voorhis, T. Time-dependent Projected Hartree-Fock. *J. Chem. Phys.* **2015**, *142*, 124103.
- (20) Joshi, A. W. *Elements of Group Theory for Physicists*; New Age International: 1997.
- (21) Tinkham, M. *Group Theory and Quantum Mechanics*; Courier Corporation: 2003.
- (22) Percus, J.; Rotenberg, A. Exact Eigenfunctions of Angular Momentum by Rotational Projection. *J. Math. Phys.* **1962**, *3*, 928–932.
- (23) Wigner, E. *Group Theory: And its Application to the Quantum Mechanics of Atomic Spectra*; Academic Press: 1959.
- (24) Corbett, J. A Note on Angular Momentum Projection Operators. *Nucl. Phys. A* **1971**, *169*, 426–428.
- (25) Li, X.; Valeev, E. F.; Williams-Young, D.; Ding, F.; Liu, H.; Goings, J.; Petrone, A.; Lestrangle, P. *Chronus Quantum*, Beta Version; 2016; <http://www.chronusquantum.org>.
- (26) Yershova, A.; Jain, S.; LaValle, S. M.; Mitchell, J. C. Generating Uniform Incremental Grids on SO(3) Using the Hopf Fibration. *Int. J. Rob. Res.* **2010**, *29*, 801–812.
- (27) Lebedev, V. I. Values of the Nodes and Weights of Ninth to Seventeenth Order Gauss-Markov Quadrature Formulae Invariant Under the Octahedron Group with Inversion. *USSR Comp. Mater. Mater. Phys.* **1975**, *15*, 44–51.
- (28) Becke, A. D. A Multicenter Numerical Integration Scheme for Polyatomic Molecules. *J. Chem. Phys.* **1988**, *88*, 2547–2553.
- (29) Hehre, W. J.; Ditchfield, R.; Pople, J. A. Self-Consistent Molecular Orbital Methods. XII. Further Extensions of Gaussian-Type Basis Sets for Use in Molecular Orbital Studies of Organic Molecules. *J. Chem. Phys.* **1972**, *56*, 2257–2261.
- (30) Frisch, M. J.; Trucks, G. W.; Schlegel, H. B.; Scuseria, G. E.; Robb, M. A.; Cheeseman, J. R.; Scalmani, G.; Barone, V.; Petersson, G. A.; Nakatsuji, H.; Li, X.; Caricato, M.; Marenich, A. V.; Bloino, J.; Janesko, B. G.; Gomperts, R.; Mennucci, B.; Hratchian, H. P.; Ortiz, J. V.; Izmaylov, A. F.; Sonnenberg, J. L.; Williams-Young, D.; Ding, F.; Lipparini, F.; Egidi, F.; Goings, J.; Peng, B.; Petrone, A.; Henderson, T.; Ranasinghe, D.; Zakrzewski, V. G.; Gao, J.; Rega, N.; Zheng, G.; Liang, W.; Hada, M.; Ehara, M.; Toyota, K.; Fukuda, R.; Hasegawa, J.; Ishida, M.; Nakajima, T.; Honda, Y.; Kitao, O.; Nakai, H.; Vreven, T.; Throssell, K.; Montgomery, J. A., Jr.; Peralta, J. E.; Ogliaro, F.; Bearpark, M. J.; Heyd, J. J.; Brothers, E. N.; Kudin, K. N.; Staroverov, V. N.; Keith, T. A.; Kobayashi, R.; Normand, J.; Raghavachari, K.; Rendell, A. P.; Burant, J. C.; Iyengar, S. S.; Tomasi, J.; Cossi, M.; Millam, J. M.; Klene, M.; Adamo, C.; Cammi, R.; Ochterski, J. W.; Martin, R. L.; Morokuma, K.; Farkas, O.; Foresman, J. B.; Fox, D. J. *Gaussian 16*, revision A.03; Gaussian Inc.: Wallingford, CT, 2016.
- (31) Schwegler, E.; Challacombe, M. Linear Scaling Computation of the Fock Matrix. III. Formation of the Exchange Matrix with Permutational Symmetry. *Theor. Chem. Acc.* **2000**, *104*, 344–349.
- (32) Reinelt, G. *The Traveling Salesman: Computational Solutions for TSP Applications*; Springer-Verlag: 1994.
- (33) Gutin, G.; Yeo, A.; Zverovich, A. Traveling Salesman Should Not be Greedy: Domination Analysis of Greedy-type Heuristics for the TSP. *Discrete Appl. Math.* **2002**, *117*, 81–86.